INTERNATIONAL JOURNAL OF NUMERICAL MODELLING: ELECTRONIC NETWORKS, DEVICES AND FIELDS
Int. J. Numer. Model. 2011; **24**:154–174
Published online 28 June 2010 in Wiley Online Library (wileyonlinelibrary.com). DOI: 10.1002/jnm.768

A practical guide to multidimensional wave digital algorithms using an example of fluid dynamics

Georg Hetmanczyk*,† and Karlheinz Ochs

Department of Electrical Engineering and Information Sciences, Ruhr-University, 44780 Bochum, Germany

SUMMARY

The wave digital concept for numerical integration of partial differential equations leads to algorithms with highly advantageous features as robustness, full localness and massive parallelism. However, the required synthesis of an internally multidimensionally passive reference circuit, from which the algorithm is derived, usually demands an in-depth knowledge of circuit theory and a high level of intuition. In this practical guide, a step-by-step approach for the synthesis of such reference circuits is introduced to relax these requirements, using the nonlinear fluid dynamic equations as a nontrivial example. General implementation issues for the wave digital algorithm are discussed as well as applying arbitrary passive linear multistep methods in place of the commonly used trapezoidal rule. As an example, we take the well-known numerically critical shock tube problem, the solution of which is problematic when the trapezoidal rule is used as unwanted oscillations occur. These oscillations are suppressed when using the second-order accurate Gear method instead. Copyright © 2010 John Wiley & Sons, Ltd.

Received 25 November 2009; Revised 13 April 2010; Accepted 16 April 2010

KEY WORDS: wave digital algorithm; numerical integration; reference circuit; fluid dynamics

1. INTRODUCTION

In recent years, the wave digital concept has been proposed for the numerical integration of partial differential equations (PDEs). It leads to algorithms with unique robustness properties, full localness and massive parallelism [1–4]. This is achieved by drawing advantage of natural properties of the modeled physical system, such as passivity resulting from energy conservation, and finite speed of propagation resulting from action at proximity. The method relies on the synthesis of an internally multidimensionally passive reference circuit equivalently describing the PDEs, which serves as reference for a one-to-one corresponding realizable wave digital algorithm. Some efforts have been made to find such reference circuits for many prominent PDEs, such as those describing fluid dynamics, electromagnetic fields, neutron diffusion, etc., cf. [4] and the references therein. However, the derivations given in the literature (if given at all) usually contain a high degree of intuition. There exist promising approaches for automating the synthesis of reference circuits for certain classes of nonlinear ordinary and linear PDEs [5, 6].

This paper is intended as a complete and practical guide to nonlinear multidimensional wave digital models from manual circuit derivation aspects to issues of implementation, retaining a high level of generality. For obtaining reference circuits, we present a step-by-step procedure, which although shown here for a specific example, is in principle applicable to all of the

*Correspondence to: Georg Hetmanczyk, Department of Electrical Engineering and Information Sciences, Ruhr-University, 44780 Bochum, Germany.
†E-mail: georg.hetmanczyk@rub.de

aforementioned PDEs. The differential operator notation from [7] is introduced together with some useful properties, to greatly alleviate the notation compared with the conventional approach. We take the example of a spatially one-dimensional viscous Newtonian fluid [8–12]. The corresponding set of PDEs has moderate complexity, is nontrivial due to its nonlinearity and covers all the aspects stressed in the step-by-step approach. As an improvement to the work of Fettweis and Mengel [11, 12], we obtain an internally lossless reference circuit.

As a numerical example, we take the well-known shock tube problem [13]. In the frictionless case, sophisticated numerical integration techniques are required as the solution contains discontinuities, violating assumptions of the theory of linear multistep (LMS) methods. The trapezoidal rule is commonly used in context of the wave digital method due to its superior properties [14]; however, in this case it produces unwanted oscillations that render the solution useless. Consideration of friction can partly suppress the oscillations for sufficiently small step sizes [12]. Here, we follow the approach of Hetmanczyk and Ochs [15] in greater detail and show how to implement arbitrary passive LMS methods in multidimensional wave digital models. For the shock tube problem, we demonstrate that regardless of the presence of friction, oscillations are suppressed when the second-order accurate Gear method is used, and that the computational effort can be drastically reduced compared with the former approach.

The remainder of the paper is organized as follows. We start with a brief motivation for passive modeling in Section 2. The general inductance and its special differential form are recapitulated in Section 3, and a differential operator is introduced together with some useful properties. The coordinate transformation used to achieve multidimensional causality and passivity is covered in Section 4. In Section 5, the fluid dynamic PDEs under consideration are briefly introduced. We present the step-by-step procedure and derive the reference circuit for the fluid dynamic equations in Section 6. Afterwards, wave digital realizations are discussed in Section 7, where we place special emphasis on the approximation of an inductance and the generalization from the trapezoidal rule to arbitrary passive LMS methods. The wave digital algorithm for the fluid dynamic equations is given in Section 8 together with a program flow diagram and a discussion of specific implementation issues. In Section 9, initial and boundary conditions are briefly discussed, and numerical examples are given in Section 10. Finally, conclusions are drawn in Section 11.

2. A MOTIVATION FOR PASSIVE MODELING

The wave digital concept exploits the fact that arbitrary compositions of passive systems again result in passive systems, which are known to possess good stability properties [16]. Moreover, wave digital models preserve the stability and satisfy a catalog of robustness criteria, even under finite word length conditions [3]. Such a feature is not only important for long-term simulations, but specifically in feedback systems, e.g. when the wave digital model acts as an observer [17].

For compositions of stable systems, the situation is different. Consider the simple example of Figure 1, where an FIR filter is involved in a feedback loop with a system consisting of a multiplier ρ whose absolute value is smaller than 1. Both systems are obviously asymptotically stable. However, the resulting system is unstable for $0.5<\rho<1$, which can be verified by computing poles of the resulting transfer function or, for instance, the step response. As opposed to passive systems, stability properties need to be reassessed. We emphasize that this can be particularly difficult for nonlinear systems.

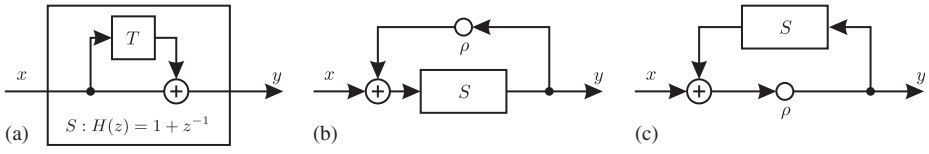

Figure 1. (a) FIR-filter (asymptotically stable) and (b), (c) unstable due to feedback even for $0.5<\rho\leqslant 1$.

DOI: 10.1002/jnm

3. GENERAL INDUCTANCE

3.1. Introduction

When synthesizing an electrical circuit for a given set of differential equations, differential expressions of a variant and nonlinear nature may have to be regarded. Even then, the circuit should model physically passive components in a passive manner. This demand motivates the definition of a general inductance [4, 18]. It can be derived by a composition of an energy neutral transformer, whose turns ratio $n \geqslant 0$ reflects any variability, and a constant inductance L_0, see Figure 2. Evidently, passivity is guaranteed if and only if $L_0 \geqslant 0$. Using the equations

$$u_0 = L_0 \frac{\mathrm{d}i_0}{\mathrm{d}t}, \quad u = u_0 n \quad \text{and} \quad i = i_0/n, \tag{1}$$

the voltage–current relationship can be formulated as

$$u = \sqrt{L}\frac{\mathrm{d}}{\mathrm{d}t}(\sqrt{L}i), \tag{2}$$

where $L = n^2 L_0$. The power and energy thus read

$$p = \sqrt{L}i\frac{\mathrm{d}}{\mathrm{d}t}(\sqrt{L}i) = \frac{1}{2}\frac{\mathrm{d}}{\mathrm{d}t}(Li^2) \quad \text{and} \quad E = \frac{1}{2}Li^2, \tag{3}$$

and an inductance of form (2) is passive if and only if $L \geqslant 0$. As indicated in [4], this is not the case for other definitions such as $u = L\mathrm{d}i/\mathrm{d}t$ or $u = \mathrm{d}Li/\mathrm{d}t$; therefore, we use the form (2) throughout this paper. A capacitance can be treated in the same way with interchanged roles of u and i.

Usually, the differential expressions of a given set of differential equations are not of the form (2) and have to be reformulated. One possibility is to solve the equation

$$f(i)\frac{\mathrm{d}}{\mathrm{d}t}g(i) = \sqrt{L(i)}\frac{\mathrm{d}}{\mathrm{d}t}(\sqrt{L(i)}i), \tag{4}$$

which leads to

$$L(i) = \frac{2}{i^2}\int_{g_0}^{g} i f(i)\,\mathrm{d}g \quad \text{with } \mathrm{d}g = \frac{\mathrm{d}g}{\mathrm{d}t}\mathrm{d}t \quad \text{and} \quad g_0 = g(i(t_0)) \tag{5}$$

under the assumption $E(t_0) = 0$, i.e. the initial energy of the inducance vanishes. The integral in (5) needs $if(i)$ to be represented as a function of g. For the special case $g(i) = i$ and $f(i) = i^m$ we obtain

$$L(i) = \frac{2i^m}{m+2} \quad \text{i.e. } i^m\frac{\mathrm{d}i}{\mathrm{d}t} = \sqrt{\frac{2i^m}{m+2}}\frac{\mathrm{d}}{\mathrm{d}t}\left(\sqrt{\frac{2i^m}{m+2}}i\right). \tag{6}$$

Evidently, the form (2) may easily lead to bulky expressions. We therefore introduce a differential operator that greatly alleviates the notation, and discuss some useful properties in order to simplify the reformulation of differential expressions.

3.2. A generalized differential operator

For application to PDEs, the results presented are generalized to multiple coordinates by substituting $\mathrm{d}/\mathrm{d}t$ with any partial derivative, e.g. $\partial/\partial\xi$. Furthermore, we use the differential

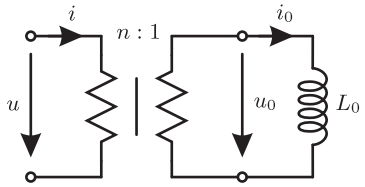

Figure 2. Representation of a general inductance as a composition of an ideal transformer and a constant inductance.

DOI: 10.1002/jnm

operator

$$\mathscr{D}_\xi\{L,i\} = \sqrt{L}\frac{\partial}{\partial\xi}(\sqrt{L}i) \tag{7}$$

for the remainder of this paper, where ξ indicates the respective coordinate. The operator specifies the voltage of a general inductance in the above context, and may of course be used to describe general capacitances as well.

Most of the properties presented in the following are commonly used in the context of the general inductance, cf. [4]; however, we place emphasis on the usage of (7). With this operator, differential expressions can directly be rewritten as:

$$\frac{\partial i}{\partial\xi} = \mathscr{D}_\xi\{1,i\} = 2\mathscr{D}_\xi\{i,1\}. \tag{8a}$$

Moreover, the following rules are essential for the manipulation of differential expressions:

$$\mathscr{D}_\xi\{\alpha L,i\} = \sqrt{\alpha}\mathscr{D}_\xi\{L,\sqrt{\alpha}i\}, \tag{8b}$$

$$\mathscr{D}_\xi\{L,i\} = \frac{i}{2}\mathscr{D}_\xi\{1,\ L\}+LD_\xi\{1,\ i\}, \tag{8c}$$

$$\mathscr{D}_\xi\{L,i\} = \frac{1}{2}(L\mathscr{D}_\xi\{1,\ i\}+\mathscr{D}_\xi\{1,\ Li\}). \tag{8d}$$

Proof of the above relationships is obtained with the definition (7) and manipulations involving the product rule and chain rule. The differential operator exhibits homogeneity in both arguments,

$$\alpha\mathscr{D}_\xi\{L,i\} = \mathscr{D}_\xi\{\alpha L,i\} = \mathscr{D}_\xi\{L,\alpha i\} \quad \text{for } \frac{\partial\alpha}{\partial\xi} = 0, \tag{8e}$$

as well as additivity,

$$\mathscr{D}_\xi\{L_1,i\}+\mathscr{D}_\xi\{L_2,i\} = \mathscr{D}_\xi\{L_1+L_2,i\} \quad \text{and} \tag{8f}$$

$$\mathscr{D}_\xi\{L,i_1\}+\mathscr{D}_\xi\{L,i_2\} = \mathscr{D}_\xi\{L,i_1+i_2\}, \tag{8g}$$

which is verified using (7) and the identity (8c). Linearity in both arguments follows. We also consider a linear combination of differential operators

$$\alpha\mathscr{D}_{\xi_1}\{L,i\}+\beta\mathscr{D}_{\xi_2}\{L,i\} = \mathscr{D}_{\xi_{12}}\{L,i\} \quad \text{with } \mathscr{D}_{\xi_{12}} = [\alpha\mathscr{D}_{\xi_1}+\beta\mathscr{D}_{\xi_2}], \tag{8h}$$

where α and β are constant and $\mathscr{D}_{\xi_{12}}$ refers to a new coordinate direction. This is needed for achieving multidimensional causality in Section 4. In Figure 3, electrical representations of some of the above rules are given, which are useful for direct circuit manipulations.

Finally, we consider a coupling of two differential equations. The involved terms should be of the symmetric form

$$\begin{aligned} u_1 &= [\mathscr{D}_{\xi_1} - \mathscr{D}_{\xi_2}]\{L,i_2\} = \mathscr{D}_{\xi_1}\{L,i_1+i_2\}+\mathscr{D}_{\xi_2}\{L,i_1-i_2\}+[\mathscr{D}_{\xi_1}+\mathscr{D}_{\xi_2}]\{-L,i_1\},\\ u_2 &= [\mathscr{D}_{\xi_1} - \mathscr{D}_{\xi_2}]\{L,i_1\} = \mathscr{D}_{\xi_1}\{L,i_2+i_1\}+\mathscr{D}_{\xi_2}\{L,i_2-i_1\}+[\mathscr{D}_{\xi_1}+\mathscr{D}_{\xi_2}]\{-L,i_2\}, \end{aligned} \tag{8i}$$

which is commonly realized by the two-port in the last row of Figure 3. Its advantage lies in a very efficient implementation in the final algorithm, presented later in this paper. Notice that the occuring negative inductances need to be combined with positive inductances of high enough value to achieve internal passivity of the circuit.

4. COORDINATE TRANSFORMATION

As a fundamental requirement, a physical model described by given PDEs exhibits causality with respect to the time variable t. Attempting to obtain a reference circuit using the given coordinates usually leads to general inductances with associated differential operator $\mathscr{D}_t$ and ones associated with a purely spatial direction, e.g. $\mathscr{D}_x$. However, causality is not given for spatial coordinates. As the concept of passivity is based on causality, we require the physical

DOI: 10.1002/jnm

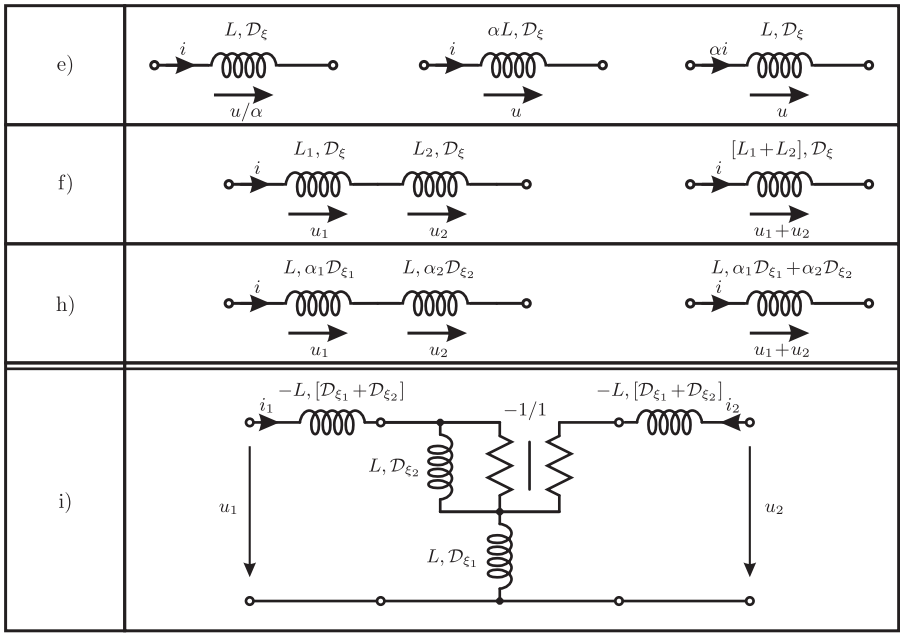

Figure 3. Electrical interpretations for expressions involving the differential operator $\mathscr{D}$.

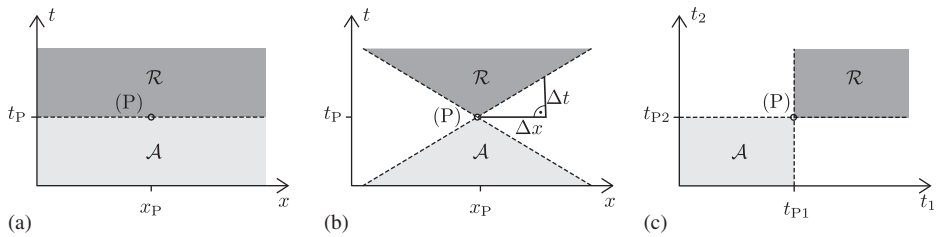

Figure 4. (a) Physical causality; (b) physical causality and finite propagation speed $v_1 = \Delta x/\Delta t$ (which is assumed to be constant in the diagram for simplicity); and (c) multidimensional causality.

system to be causal with respect to all coordinates it is described in. This can be achieved for systems with finite propagation speed, using the transformation approach [4] presented in this section.

Physical causality is illustrated in Figure 4(a): the domain of action $\mathscr{A}$ of a point P with spatial coordinate x_P and temporal coordinate t_P encompasses all coordinates with $t \leqslant t_P$, the domain of reaction $\mathscr{R}$ is given by $t \geqslant t_P$. This implies the possibility of infinite propagation speed, which is a contradiction to the principle of action at proximity. A realistic physical model should imply finite propagation speed, as information needs time to overcome a spatial distance. This is illustrated in Figure 4(b) for a constant propagation velocity. Figure 4(c) depicts *multidimensional* causality: Coordinates are chosen such that the domains of action $\mathscr{A}$ and reaction $\mathscr{R}$ are given by:

$$\mathscr{A} = \{t_1 \leqslant t_{1P}, t_2 \leqslant t_{2P}\} \quad \text{and} \quad \mathscr{R} = \{t_1 \geqslant t_{1P}, t_2 \geqslant t_{2P}\}. \tag{9}$$

Each of the new coordinates now has the meaning of time. It is evident that the domains in Figure 4(b) can be mapped bijectively to the ones in Figure 4(c) by scaling the time coordinate and applying a rotation.

In the following, we assume k old coordinates comprised of $k-1$ spatial coordinates $x_1, \ldots, x_{k-1}$ and the time coordinate t. We further assume k' new time coordinates $t_1, \ldots, t_{k'}$, with $k' \geqslant k$. The case $k' > k$ is useful for later discretization and can be interpreted as embedding into a

DOI: 10.1002/jnm

higher-dimensional system [2]. The warped time variable

$$x_k = x_k(t), \quad v_k(t) = \frac{\mathrm{d}x_k}{\mathrm{d}t} > 0, \tag{10}$$

can be a function adapting to a possibly variant propagation speed (as in the case of fluid dynamic problems). The vectors of coordinates are defined by:

$$\boldsymbol{x} = [x_1, \ldots, x_k]^{\mathrm{T}} \quad \text{and} \quad \boldsymbol{t} = [t_1, \ldots, t_{k'}]^{\mathrm{T}}. \tag{11a, b}$$

The old and new coordinates are related by a linear transformation

$$\boldsymbol{x} = v_0 \boldsymbol{H} \boldsymbol{t}, \quad \boldsymbol{t} = \frac{1}{v_0} \boldsymbol{H}^{-\mathrm{R}} \boldsymbol{x}, \tag{12a, b}$$

with transformation matrix $\boldsymbol{H} \in \mathbb{R}^{k,k'}$ and a suitably chosen right inverse $\boldsymbol{H}^{-\mathrm{R}}$. The constant scaling factor v_0 is positive and ensures proper physical dimensions. We further introduce the vectors of frequency variables with respect to the old and new coordinates,

$$\boldsymbol{p}_{\boldsymbol{x}} = [p_{x_1}, \ldots, p_{x_k}]^{\mathrm{T}} \quad \text{and} \quad \boldsymbol{p}_{\boldsymbol{t}} = [p_{t_1}, \ldots, p_{t_{k'}}]^{\mathrm{T}}, \tag{13a, b}$$

for which the following relationships hold:

$$\boldsymbol{p}_{\boldsymbol{x}}^{\mathrm{T}} \boldsymbol{x} = \boldsymbol{p}_{\boldsymbol{t}}^{\mathrm{T}} \boldsymbol{t} \quad \text{and} \quad \boldsymbol{p}_{\boldsymbol{t}} = v_0 \boldsymbol{H}^{\mathrm{T}} \boldsymbol{p}_{\boldsymbol{x}}. \tag{14a, b}$$

As we will later be interested in the transformation of general inductances, we also formally define the generalized differential operators according to (7),

$$\mathscr{D}_{\boldsymbol{x}} = [\mathscr{D}_{x_1}, \ldots, \mathscr{D}_{x_k}]^{\mathrm{T}} \quad \text{with} \quad \mathscr{D}_{x_\kappa}\{L, i\} = \sqrt{L} \frac{\partial}{\partial x_\kappa} (\sqrt{L} i), \quad \kappa = 1, \ldots, k \quad \text{and} \tag{15a}$$

$$\mathscr{D}_{\boldsymbol{t}} = [\mathscr{D}_{t_1}, ..., \mathscr{D}_{t_{k'}}]^{\mathrm{T}} \quad \text{with} \quad \mathscr{D}_{t_\kappa}\{L, i\} = \sqrt{L} \frac{\partial}{\partial t_\kappa} \left(\sqrt{L} i \right), \quad \kappa = 1, \ldots, k'. \tag{15b}$$

The temporal differential operator is transformed by

$$\frac{\partial}{\partial t} = \frac{\mathrm{d}x_k}{\mathrm{d}t} \frac{\partial}{\partial x_k} \quad \text{i.e. } \mathscr{D}_t\{L, i\} = \sqrt{L} \frac{\partial}{\partial t} \sqrt{L} i = v_k(t) \mathscr{D}_{x_k}\{L, i\}, \tag{16}$$

cf. (10). Moreover, using the respective Jacobian of the transformations (12) and regarding the results in Section 3.2, we find the relation between the differential operators

$$\mathscr{D}_{\boldsymbol{x}} = \frac{1}{v_0} \boldsymbol{H}^{-\mathrm{RT}} \mathscr{D}_{\boldsymbol{t}}, \quad \mathscr{D}_{\boldsymbol{t}} = v_0 \boldsymbol{H}^{\mathrm{T}} \mathscr{D}_{\boldsymbol{x}}. \tag{17a, b}$$

The above formulas serve for the transformation of the PDEs at hand. In particular, (17a) is used to express old differential operators by the new ones.

5. SPATIALLY ONE-DIMENSIONAL EQUATIONS OF A FLUID

The spatially one-dimensional equations of a fluid with velocity v, pressure p, mass density ρ, internal energy density e_i and negative stress w read, in a commonly used form, as follows:

$$\rho \left(\frac{\partial v}{\partial t} + v \frac{\partial v}{\partial x} \right) + \frac{\partial p}{\partial x} = f \quad \text{with} \quad f = -\frac{\partial w}{\partial x}, \tag{18a}$$

$$\frac{\partial e_{\mathrm{i}}}{\partial t} + \frac{\partial v e_{\mathrm{i}}}{\partial x} + p \frac{\partial v}{\partial x} = q_{\mathrm{f}} \quad \text{with} \quad q_{\mathrm{f}} = -w \frac{\partial v}{\partial x}, \tag{18b}$$

$$\frac{\partial \rho}{\partial t} + \frac{\partial v \rho}{\partial x} = 0, \tag{18c}$$

$$w + \eta \frac{\partial v}{\partial x} = 0. \tag{18d}$$

In the above, (18a) describes conservation of impulse and is known as Navier–Stokes equation, furthermore (18b) and (18c) describe conservation of internal energy and mass, respectively. The

DOI: 10.1002/jnm

term f models friction and the term q_f models the corresponding generated internal power. We assume a Newtonian fluid, which results in the fourth equation (18d) for w. There η is the dynamic viscosity, $\eta > 0$. Using (18d) in the right equation of (18b), the term q_f can be rewritten as:

$$q_f = \frac{w^2}{\eta}. \tag{18e}$$

Finally, a thermodynamic state equation is needed to complement the above differential equations. Throughout this paper, we assume an ideal gas

$$e_i = \frac{p}{\gamma_i - 1} \quad \text{with } 1 < \gamma_i < 2, \tag{18f}$$

where γ_i is the isentropic coefficient. The above relationship is used to eliminate e_i in (18b), remaining with four differential equations for the unknowns v, p, ρ and w, which we refer to as field quantities.

6. REFERENCE CIRCUIT FOR THE FLUID DYNAMIC EQUATIONS

The reference circuit for the fluid dynamic equations without friction is given in [9], the one regarding friction in [12]. In this section, our aim is to present a clear and structured derivation, greatly benefiting from the differential operator (7) and its properties. It is written as a step-by-step guide including all essential aspects for many further types of PDEs, including Maxwell's equations and neutron diffusion.

6.1. Ensure that the PDEs are of first order and of hyperbolic type

As inductances and capacitances in a reference circuit reflect first-order differential expressions, the PDEs to start with should also be in first-order form. This is often given directly from the physical derivation, as in the case of the fluid dynamic equations. In other instances, higher-order differential equations need to be rewritten as several first-order equations by introducing additional field quantities.

We say that the PDEs are of hyperbolic type, if the underlying physical model implies finite propagation speed of all phenomena. As indicated above, this is a fundamental requirement of the wave digital method, as it is necessary for achieving multidimensional causality, and thus, multidimensional passivity. Equation (18d) is not hyperbolic as it does not contain any derivatives with respect to time (it is of parabolic type). The common approach is to supplement an additional term making it hyperbolic, e.g.

$$l_f \frac{\partial w}{\partial t} + \frac{w}{\eta} + \frac{\partial v}{\partial x} = 0, \quad l_f > 0 \quad \text{const.} \tag{19}$$

The constant l_f is a parameter to be specified suitably later on. Evidently, the larger its value, the larger is the deviation from the original model. A value too small will result in an unnecessarily high computational effort. More specifically, as $l_f \to 0$ the parabolic case is approached, meaning that the propagation speed tends to infinity, which implies a vanishing time progress in the final integration algorithm.

Despite the above modification for hyperbolization, the overall model should still preserve energy. Therefore, we keep q_f in the left equation of (18b) for the following derivations and specify it later with help of the electric interpretation, in a way that the resulting circuit is lossless. We emphasize that this possibility is a key advantage of the electric interpretation.

6.2. Obtain differential terms interpretable as general reactive elements

Particularly for nonlinear problems, this step is probably the most difficult to complete, as there exist no general procedures. The PDEs are reformulated in a mostly non-obvious

DOI: 10.1002/jnm

manner to obtain differential terms of form (2). Even though this part of the derivation is problem-dependent, the fluid dynamic equations are an instructive example to present some methods of reformulation.

Equation (18a) can be rewritten to express conservation of kinetic energy, and this form is more suited for deriving a reference circuit due to its strong analogy to (18b). The form is obtained by adding (18a) multiplied by v to (18c) multiplied by $\frac{1}{2}v^2$ and subsequently using the product rule, leading to

$$\frac{\partial e}{\partial t}+\frac{\partial ve}{\partial x}+v\frac{\partial p}{\partial x}=-v\frac{\partial w}{\partial x} \quad \text{where } e=\tfrac{1}{2}\rho v^2 \tag{20}$$

is the kinetic energy per unit volume. The overall set of equations now represents the conservation of quantities proportional to energy. Denoted with the differential operator (7), it has the form

$$\begin{aligned}
&\mathscr{D}_t\{1,\tfrac{1}{2}\rho v^2\} + \mathscr{D}_x\{1,v\tfrac{1}{2}\rho v^2\} + v\mathscr{D}_x\{1,p\} + v\mathscr{D}_x\{1,w\} &&= 0,\\
&\mathscr{D}_t\{1,e_\mathrm{i}\} + \mathscr{D}_x\{1,ve_\mathrm{i}\} + p\mathscr{D}_x\{1,v\} &&= q_\mathrm{f},\\
&\mathscr{D}_t\{1,\rho\} + \mathscr{D}_x\{1,v\rho\} &&= 0,\\
&\mathscr{D}_t\{1,l_\mathrm{f}w\} + \frac{w}{\eta} + \mathscr{D}_x\{1,v\} &&= 0.
\end{aligned}$$

The objective is an interpretation of the above PDEs as loop equations involving general inductances.[‡] For this aim, all variant prefactors of differential operators need to be eliminated, and only four different expressions may occur as second argument of the differential operators, which will be interpreted as loop currents and represent state variables of the circuit. From these electrical state variables, the field quantities v, p, ρ and w need to be uniquely determinable. An additional property to achieve is the symmetry of coupling terms in the first argument, as it leads to the simple reciprocal coupling structure given in the last row of Figure 3. We aim at the state variables $v\sqrt{p}$, $\sqrt{p}$, $\sqrt{\rho}$ and $w\sqrt{p}$, which prove to work well for the present purpose. Note that $p>0$ and $\rho>0$ due to physical reasons. As a preparation, we make use of the relationship (8a) and perform several expansions with the term p/p, which will be splitted among the first and second argument of the differential operator:

$$\begin{aligned}
&\mathscr{D}_t\left\{\frac{\rho}{p}v^2p,1\right\} + \mathscr{D}_x\left\{\frac{v\rho}{p}v^2p,1\right\} + v\mathscr{D}_x\{2p,1\} + v\mathscr{D}_x\left\{\frac{1}{p}p,w\right\} &&= 0,\\
&\mathscr{D}_t\left\{2\frac{e_\mathrm{i}}{p}p,1\right\} + \mathscr{D}_x\left\{\frac{2ve_\mathrm{i}}{p}p,1\right\} - \mathscr{D}_x\left\{2\frac{pv}{p}p,1\right\} + \mathscr{D}_x\{2p,v\} &&= q_\mathrm{f},\\
&\mathscr{D}_t\{2\rho,1\} + \mathscr{D}_x\{2\rho v,1\} &&= 0,\\
&\mathscr{D}_t\left\{\frac{l_\mathrm{f}}{p}p,w\right\} + \frac{w}{\eta} + \mathscr{D}_x\left\{\frac{1}{p}p,v\right\} &&= 0.
\end{aligned}$$

Special attention is required for the second equation, where (8c) was used to split $p\mathscr{D}_x\{1,v\}$. In the resulting equation, the second and third term are combined using (8f). We now apply (8b) and divide the equations by $v\sqrt{p}$, $\sqrt{p}$, $\sqrt{\rho}$ and $\sqrt{p}$, respectively, to eliminate the generated

[‡]An interpretation as node equations involving general capacitances is also possible; for some applications a combination of both approaches may be feasible.

DOI: 10.1002/jnm

prefactors. As a result, we obtain a set of equations with the desired structure,

$$\begin{aligned}
&\mathscr{D}_t\left\{\frac{\rho}{p}, v\sqrt{p}\right\} + \mathscr{D}_x\left\{\frac{v\rho}{p}, v\sqrt{p}\right\} + \mathscr{D}_x\{2, \sqrt{p}\} + \mathscr{D}_x\left\{\frac{1}{p}, w\sqrt{p}\right\} &&= 0,\\
&\mathscr{D}_t\left\{\frac{2e_\mathrm{i}}{p}, \sqrt{p}\right\} + \mathscr{D}_x\left\{\frac{2v(e_\mathrm{i}-p)}{p}, \sqrt{p}\right\} + \mathscr{D}_x\{2, v\sqrt{p}\} &&= \frac{q_\mathrm{f}}{\sqrt{p}},\\
&\mathscr{D}_t\{2, \sqrt{\rho}\} + \mathscr{D}_x\left\{2v, \sqrt{\rho}\right\} &&= 0,\\
&\mathscr{D}_t\left\{\frac{l_\mathrm{f}}{p}, w\sqrt{p}\right\} + \frac{1}{p\eta}w\sqrt{p} + \mathscr{D}_x\left\{\frac{1}{p}, v\sqrt{p}\right\} &&= 0.
\end{aligned}$$

Coupling terms are given in the third and fourth column, exhibiting the formerly mentioned symmetry in the first argument.

6.3. Normalize dependent variables

Generally, the state variables are represented by voltages and currents in the reference circuit. It is thus important to normalize them to an appropriate physical dimension, such that they can be coupled with the Kirchhoff laws. As we will see later on, proper normalization also allows for optimizing the resulting circuit. Regarding the above reformulation of equations, we define

$$\begin{aligned}
&i_1(x,t) = \alpha_1(t)v(x,t)\sqrt{p(x,t)}, \quad i_2(x,t) = \alpha_2(t)\sqrt{p(x,t)},\\
&i_3(x,t) = \alpha_3(t)\sqrt{\rho(x,t)}, \qquad i_4(x,t) = \alpha_4(t)w(x,t)\sqrt{p(x,t)},
\end{aligned} \tag{21}$$

with time-variant scale functions fulfilling $\alpha_\nu > 0$, with $\nu = 1,\ldots,4$. To preserve the form (2) of general inductances upon substitution of the state variables, in each equation we divide by the respective scale function α_ν, use (8b) with $\sqrt{\alpha} = 1/\alpha_\nu$ for the first term and the homogeneity (8e) for the following terms. The result reads

$$\begin{aligned}
&\mathscr{D}_t\left\{\frac{\rho}{\alpha_1^2 p}, i_1\right\} + \mathscr{D}_x\left\{\frac{v\rho}{\alpha_1^2 p}, i_1\right\} + \mathscr{D}_x\left\{\frac{2}{\alpha_1\alpha_2}, i_2\right\} + \mathscr{D}_x\left\{\frac{1}{\alpha_1\alpha_4 p}, i_4\right\} &&= 0,\\
&\mathscr{D}_t\left\{\frac{2e_i}{\alpha_1^2 p}, i_2\right\} + \mathscr{D}_x\left\{\frac{2v(e_i-p)}{\alpha_2^2 p}, i_2\right\} + \mathscr{D}_x\left\{\frac{2}{\alpha_1\alpha_2}, i_1\right\} &&= \frac{q_\mathrm{f}}{\alpha_2\sqrt{p}},\\
&\mathscr{D}_t\left\{\frac{2}{\alpha_3^2}, i_3\right\} + \mathscr{D}_x\left\{\frac{2v}{\alpha_3^2}, i_3\right\} &&= 0,\\
&\mathscr{D}_t\left\{\frac{l_\mathrm{f}}{\alpha_4^2 p}, i_4\right\} + \frac{1}{\alpha_4^2 p\eta}i_4 + \mathscr{D}_x\left\{\frac{1}{\alpha_1\alpha_4 p}, i_1\right\} &&= 0.
\end{aligned}$$

6.4. Apply the coordinate transformation

At this stage, the system is transformed to obtain multidimensional causality and passivity. We adopt the notation of (11) and introduce the time scale by using (16). To preserve the form (2), we divide by $v_2(t)$ and use (8e). We choose the commonly used transformation matrix

$$\boldsymbol{H} = \begin{bmatrix} 1 & -1 \\ 1 & 1 \end{bmatrix}, \quad \boldsymbol{H}^{-\mathrm{R}} = \boldsymbol{H}^{-1} = \frac{1}{2}\begin{bmatrix} 1 & 1 \\ -1 & 1 \end{bmatrix}, \tag{22a, b}$$

cf. [2], and set $v_0 = 1$ for practical reasons, as this constant is in fact only relevant for theoretical considerations and yields no additional degree of freedom.[§] By making use of the abbreviations

$$\begin{aligned}
&l_{1\pm} = \frac{\rho}{2\alpha_1^2 p}\left(1 \pm \frac{v}{v_2}\right), \quad l_{2\pm} = \frac{e_\mathrm{i} \pm (e_\mathrm{i}-p)v/v_2}{\alpha_2^2 p}, \quad l_{3\pm} = \frac{1}{\alpha_3^2}\left(1 \pm \frac{v}{v_2}\right), \quad l_4 = \frac{l_\mathrm{f}}{2\alpha_4^2 p},\\
&l_{12} = \frac{1}{\alpha_1\alpha_2 v_2}, \qquad l_{14} = \frac{1}{2\alpha_1\alpha_4 v_2 p}, \qquad r_{24} = \frac{1}{\alpha_4^2 v_2 p\eta}, \qquad q_{24} = \frac{q_\mathrm{f}}{\alpha_2 v_2\sqrt{p}},
\end{aligned}$$

[§]This choice leads to equal units for $\boldsymbol{x}$ and $\boldsymbol{t}$.

DOI: 10.1002/jnm

the result has the following form:

$$\begin{array}{llllll} \mathscr{D}_{x_2}\{l_{1+}+l_{1-}, i_1\} & + \mathscr{D}_{x_1}\{l_{1+}-l_{1-},\, i_1\} & + 2\mathscr{D}_{x_1}\{l_{12},\, i_2\} & + 2\mathscr{D}_{x_1}\{l_{14},\, i_4\} & = & 0, \\ \mathscr{D}_{x_2}\{l_{2+}+l_{2-}, i_2\} & + \mathscr{D}_{x_1}\{l_{2+}-l_{2-},\, i_2\} & + 2\mathscr{D}_{x_1}\{l_{12},\, i_1\} & & = & q_{24}, \\ \mathscr{D}_{x_2}\{l_{3+}+l_{3-}, i_3\} & + \mathscr{D}_{x_1}\{l_{3+}-l_{3-},\, i_3\} & & & = & 0, \\ 2\mathscr{D}_{x_2}\{l_4, i_4\} & + r_{24} i_4 & + & 2\mathscr{D}_{x_1}\{l_{14},\, i_1\} & = & 0. \end{array}$$

The differential operators are substituted with (17a) and sorted using (8f) and (8h). We now have the final result

$$\mathscr{D}_{t_1}\{l_{1+},\, i_1\} + \mathscr{D}_{t_2}\{l_{1-},\, i_1\} + [\mathscr{D}_{t_1}-\mathscr{D}_{t_2}]\{l_{12},\, i_2\} + [\mathscr{D}_{t_1}-\mathscr{D}_{t_2}]\{l_{14},\, i_4\} = 0, \quad (23a)$$

$$\mathscr{D}_{t_1}\{l_{2+},\, i_2\} + \mathscr{D}_{t_2}\{l_{2-},\, i_2\} + [\mathscr{D}_{t_1}-\mathscr{D}_{t_2}]\{l_{12},\, i_1\} = q_{24}, \quad (23b)$$

$$\mathscr{D}_{t_1}\{l_{3+},\, i_3\} + \mathscr{D}_{t_2}\{l_{3-},\, i_3\} = 0, \quad (23c)$$

$$\mathscr{D}_{t_1}\{l_4,\, i_4\} + \mathscr{D}_{t_2}\{l_4,\, i_4\} + r_{24} i_4 + [\mathscr{D}_{t_1}-\mathscr{D}_{t_2}]\{l_{14},\, i_1\} = 0, \quad (23d)$$

suitable for deriving a multidimensionally causal and passive reference circuit, from which a computable wave digital algorithm can be obtained.

6.5. Find reference circuit

Equation (23) can now be interpreted as loop equations involving general inductances. By construction, the currents i_1 and i_2 are coupled by the same inductance l_{12}, $[\mathscr{D}_1 - \mathscr{D}_2]$ in both (23a) and (23b). A similar situation holds for the currents i_1 and i_4 in (23a) and (23d). This type of coupling can be realized with the two-port given in the last row of Figure 3, which has a highly beneficial wave digital realization presented later on. It exhibits two negative inductances, which have to be combined with positive inductances in the respective loop equation to obtain internal passivity.

Determination of the term q_{24} is now in order. The term $r_{24} i_4$ in (23d) represents the voltage of a resistance r_{24}, which reflects the effect of friction. To achieve losslessness of the overall circuit, q_{24} was formerly interpreted as a controlled voltage source [12], cf. Figure 5(a), which feeds the power dissipated by the resistance r_{24}:

$$r_{24} i_4^2 - q_{24} i_2 \stackrel{!}{=} 0 \quad \Rightarrow \quad q_\mathrm{f} = \frac{w^2}{\eta}. \quad (24)$$

This result coincides with the classical expression (18e). Indeed, for $l_\mathrm{f} \to 0$, the power supplied is the power mechanically dissipated. A disadvantage of this realization is that the losslessness is only given externally, as a source is involved. We therefore suggest the realization of Figure 5(b), which features a nonlinear gyrator and is internally lossless.

The overall circuit is depicted in Figure 6, where each of the loops represents one of the formulas (23a–d). There, the inductances are given by:

$$l_{v\pm} = l_{1\pm} - l_{12} - l_{14}, \quad l_{p\pm} = l_{2\pm} - l_{12}, \quad l_{\rho\pm} = l_{3\pm}, \quad l_w = l_4 - l_{14}.$$

6.6. Circuit optimization and passivity considerations

There are six degrees of freedom in the derived circuit, α_v with $v = 1, \ldots, 4$, l_f and v_2. The standard approach is now to derive inequalities for the parameters from multidimensional causality and internal multidimensional passivity constraints, and then attempt to optimize the

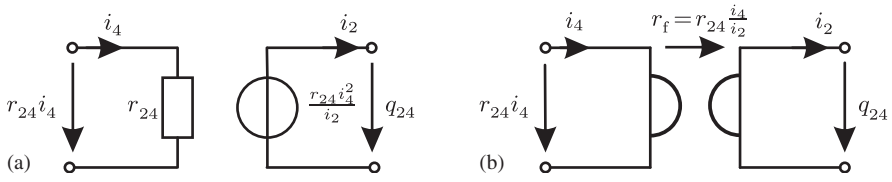

Figure 5. Realization of the friction terms: (a) with resistance and source and (b) internally lossless.

DOI: 10.1002/jnm

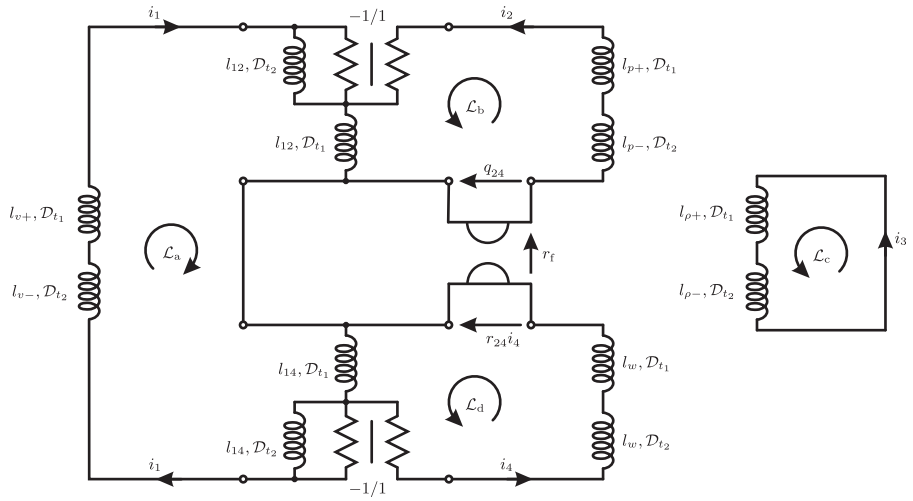

Figure 6. Reference circuit for the fluid dynamic equations.

circuit in the sense that the time scale $v_2(t)$ is minimized, while as many elements as possible are eliminated.

In the present case, this procedure leads to intractable expressions. Therefore, we adopt the opposite way and eliminate α_2, α_3 and α_4 by simplifying the circuit, keep l_f as a design parameter for hyperbolization, and obtain simple restrictions for the remaining two parameters by passivity considerations.

First, we choose $\alpha_3 = 1$ as it has no influence on any coupling terms. Next, the inductance l_w can be eliminated

$$l_w = 0 \quad \Leftrightarrow \quad l_4 = l_{14} \quad \Leftrightarrow \quad \alpha_4 = \alpha_1 v_2 l_f. \tag{25}$$

Note that this is not possible for $l_{p\pm}$ as $l_{2\pm}$ is spatially variant, while l_{12} is not. A similar situation holds for $l_{v\pm}$. We eliminate one more degree of freedom by choosing l_{12} to be constant

$$l_{12} = 1 \quad \Leftrightarrow \quad \alpha_2 = \frac{1}{\alpha_1 v_2}. \tag{26}$$

Now, all normalized inductances are dimensionless. For this reason, we introduce the abbreviation

$$p_f := \frac{1}{2\alpha_1\alpha_4 v_2} = \frac{1}{2\alpha_1^2 v_2^2 l_f} \quad \Rightarrow \quad l_{14} = \frac{p_f}{p}, \tag{27}$$

which we use instead of α_1. The element values have the final form

$$\begin{aligned} l_{v\pm} &= \frac{v_2^2 l_f p_f \rho}{p}\left(1 \pm \frac{v}{v_2}\right) - 1 - \frac{p_f}{p}, \quad l_{p\pm} = \frac{1}{2 l_f p_f p}\left[e_i \pm (e_i - p)\frac{v}{v_2}\right] - 1, \\ l_{\rho\pm} &= 1 \pm \frac{v}{v_2}, \quad l_{12} = 1, \quad l_{14} = \frac{p_f}{p}, \quad r_f = \frac{w}{l_f v_2 \eta p}. \end{aligned} \tag{28}$$

Next, we obtain conditions for the time scale by requiring internal multidimensional passivity. We start with

$$l_{v\pm} \geqslant 0 \quad \text{and} \quad l_{\rho\pm} \geqslant 0 \quad \Leftrightarrow \quad v_2^2 \pm v v_2 - \frac{p + p_f}{l_f p_f \rho} \geqslant 0 \quad \text{and} \quad v_2 \geqslant v. \tag{29}$$

The inequalities have to be satisfied in the whole computation domain. Therefore, we introduce the global extremal values

$$v_{\max}(t) = \max_x |v(x,t)|, \quad p_{\max}(t) = \max_x p(x,t), \quad \rho_{\min}(t) = \min_x \rho(x,t), \tag{30}$$

DOI: 10.1002/jnm

to write down a sufficient condition for multidimensional passivity

$$v_2(t) \geqslant \frac{v_{\max}}{2} + \sqrt{\frac{v_{\max}^2}{4} + \frac{p_{\max} + p_{\mathrm{f}}}{l_{\mathrm{f}} p_{\mathrm{f}} \rho_{\min}}}. \tag{31}$$

The condition is, in general, not necessary as the extremal values may not occur simultaneously at the same spatial coordinate. In the above, we assume the condition $v_2 \geqslant \hat{v}$ for multidimensional causality is satisfied, where $\hat{v}$ is the maximum propagation velocity of the hyperbolized system, cf. [4]. To establish a condition for p_{f}, we regard $e_{\mathrm{i}} - p > 0$ due to (18f) and require

$$l_{p\pm} \geqslant 0 \quad \Leftrightarrow \quad \frac{e_{\mathrm{i}} - 2 l_{\mathrm{f}} p_{\mathrm{f}} p}{e_{\mathrm{i}} - p} \geqslant \pm \frac{v}{v_2}. \tag{32}$$

A sufficient condition for p_{f} assuming $v_2 \geqslant v_{\max}$ is then

$$2 l_{\mathrm{f}} p_{\mathrm{f}} \leqslant 1. \tag{33}$$

All other inductances in the reference circuit are nonnegative without further restrictions. It remains to choose an optimal value for l_{f}: The larger the value, the more severe is the influence of hyperbolization and thus the deviation from the original set of PDEs. The smaller the value, the larger v_2 has to be chosen, cf. (31), which increases computation time.

7. WAVE DIGITAL REALIZATIONS

Conservation of energy in the physical model is reflected by the circuit of Figure 6 as it contains lossless elements throughout. The circuit serves as a feasible decomposition of the original set of PDEs, in the way that the elements can be substituted by known wave digital realizations [19], which preserve the passivity element-wise. Beside the well-known robustness features [4], the resulting wave digital algorithm is semi-explicitly computable, i.e. it is explicitly computable except for the resolution of nonlinearities, while this resolution can be performed for each grid point individually.

For each port of an element, wave quantities a and b are used instead of u and i. Throughout this paper, we use power waves

$$a = \frac{u + Ri}{2\sqrt{R}}, \quad b = \frac{u - Ri}{2\sqrt{R}}, \tag{34}$$

with positive port resistance R. The nonreactive (algebraic) elements appearing in the presented circuit are series connections, the gyrator and Jaumann-structures. The reactive part, representing the differential expressions, is composed of general inductances. In the following, we briefly touch upon the wave digital realization of a differential transformer, which is a generalization of a Jaumann structure, since it is not consistently covered in the literature as opposed to the other elements [19]. Afterwards, we focus on the general inductance and revisit the approach of [15] as a generalization of the usual approximation by the trapezoidal rule.

7.1. Realization of a differential transformer

The differential transformer of Figure 7(a) with positive parameter m is a Jaumann structure for $m = 1$. Its notation varied over the years, but now seems to have reached consent. For the special choice of port resistances

$$\begin{aligned} R_1 &= (m+1)R, \quad R_3 = R, \\ R_2 &= m(m+1)R, \quad R_4 = mR, \end{aligned} \tag{35}$$

the relationship in terms of waves is particularly simple:

$$\begin{aligned} b_1 &= \alpha a_3 + \beta a_4, \quad b_3 = \alpha a_1 - \beta a_2, \\ b_2 &= -\beta a_3 + \alpha a_4, \quad b_4 = \beta a_1 + \alpha a_2, \end{aligned} \tag{36}$$

DOI: 10.1002/jnm

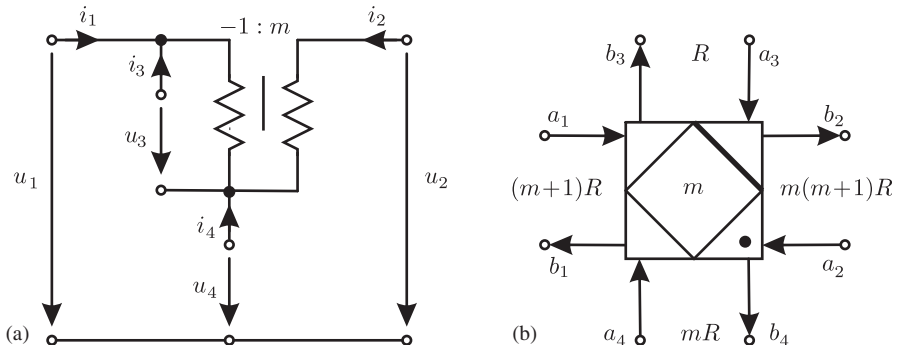

Figure 7. (a) Differential transformer and (b) differential adaptor.

where we have introduced the parameters

$$\alpha = \frac{1}{\sqrt{m+1}}, \quad \beta = \sqrt{\frac{m}{m+1}} \quad \text{with } \alpha^2+\beta^2 = 1. \tag{37}$$

The resulting wave digital equivalent is called differential adaptor [11], its symbol is shown in Figure 7. Numbering of ports is uniquely determined by the position of the dot and bold line. The designation of m is usually omitted for $m = 1$. The element is particularly useful for the realization of coupling terms as in the last row of Figure 3, since for the choice of port resistances given above, all ports are reflection free, and ports 1 and 2 as well as 3 and 4 are decoupled.

7.2. Realization of an inductance

Reactive elements, such as the general inductance, express differential relations and thus need to be approximated for discretization. In the following, we consider a constant, but multi-dimensional inductance similar to (1),

$$\tilde{u}_0(\boldsymbol{t}) = \mathscr{D}_{t_\kappa}\{L_0, \tilde{\imath}_0(\boldsymbol{t})\} = L_0 \frac{\partial}{\partial t_\kappa} \tilde{\imath}_0(\boldsymbol{t}), \quad L_0 > 0, \text{ const.} \tag{38}$$

As in Figure 2, we regard variability separately with a transformer, which can later be implemented very easily in terms of waves.

7.2.1. Approximation with the trapezoidal rule. Within the wave digital concept, approximation of differential expressions is usually done with the trapezoidal rule due to its superior stability and accuracy properties [14]. Applied to the multidimensional inductance defined by (38), it reads [4]

$$\tilde{u}_0(\boldsymbol{t}) + \tilde{u}_0(\boldsymbol{t} - \boldsymbol{T}_\kappa) = \frac{2L_0}{T}[\tilde{\imath}_0(\boldsymbol{t}) - \tilde{\imath}_0(\boldsymbol{t} - \boldsymbol{T}_\kappa)], \tag{39}$$

where we have expressed a step with size T along t_κ by the shift vector $\boldsymbol{T}_\kappa = \boldsymbol{e}_\kappa T$, with $\boldsymbol{e}_\kappa$ being a unit vector of proper dimension. In the above, we have denoted the approximated quantities in the same way as the exact ones. For implementation of the final algorithm, the original coordinates (11a) are more suited as independent variables, since these are the coordinates in which the original problem is given, including initial and boundary conditions. Using $u_0(\boldsymbol{x}) = \tilde{u}_0(\boldsymbol{t})$ and $i_0(\boldsymbol{x}) = \tilde{\imath}_0(\boldsymbol{t})$, the approximation (39) can be reformulated as

$$u_0(\boldsymbol{x}) + u_0(\boldsymbol{x} - \boldsymbol{X}_\kappa) = \frac{2L_0}{T}[i_0(\boldsymbol{x}) - i_0(\boldsymbol{x} - \boldsymbol{X}_\kappa)], \tag{40}$$

where we have expressed the shift vector by

$$\boldsymbol{X}_\kappa = v_0 \boldsymbol{H} \boldsymbol{T}_\kappa = \boldsymbol{h}_\kappa X \quad \text{with } X = v_0 T, \quad \boldsymbol{h}_\kappa = \boldsymbol{H}\boldsymbol{e}_\kappa, \tag{41}$$

DOI: 10.1002/jnm

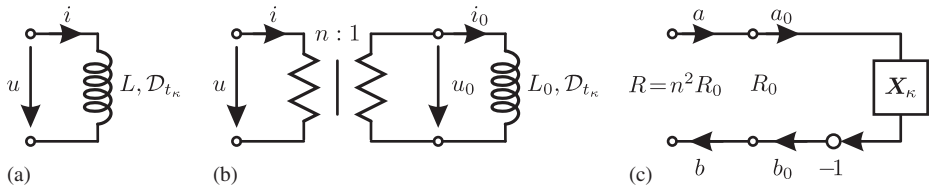

Figure 8. (a) General inductance; (b) decomposition into a transformer with variant turns ratio n and a constant inductance; and (c) wave digital realization using the trapezoidal rule, expressed in original coordinates.

cf. (12a). In the above, $\boldsymbol{h}_\kappa$ is the column κ of $\boldsymbol{H}$. Choosing a suited port resistance, the trapezoidal rule leads to a particularly simple relationship in wave variables,

$$b_0(\boldsymbol{x}) = -a_0(\boldsymbol{x} - \boldsymbol{X}_\kappa) \quad \text{with } R_0 = \frac{2L_0}{T}. \tag{42}$$

Along with the electrical representations, the resulting wave flow diagram for the general inductance including variability is depicted in Figure 8. Owing to the usage of power waves, the transformer can directly be incorporated into the port resistance without further modifications, i.e. $R = n^2 R_0 = 2L/T$ is used. The realization clearly exhibits a cause–effect relation and is, in contrast to (40), explicit. Note that applying the trapezoidal rule to a constant multidimensional capacitance defined in analogy to (38) leads to $b_0(\boldsymbol{x}) = a_0(\boldsymbol{x} - \boldsymbol{X}_\kappa)$ with $R_0 = T/(2C_0)$, and a transformer regarding variability can be incorporated in the same way.

Separation of the variability allows for a frequency domain description, for which we substitute, cf. (13),

$$u_0(\boldsymbol{x}) = U_0 \mathrm{e}^{\boldsymbol{p}_x^{\mathrm{T}} \boldsymbol{x}} \quad \text{and} \quad i_0(\boldsymbol{x}) = I_0 \mathrm{e}^{\boldsymbol{p}_x^{\mathrm{T}} \boldsymbol{x}}, \tag{43}$$

with the complex amplitudes U_0 and I_0. Using the relationships (14b) and (41), we find

$$\boldsymbol{p}_x^{\mathrm{T}} \boldsymbol{X}_\kappa = v_0 \boldsymbol{p}_x^{\mathrm{T}} \boldsymbol{H} \boldsymbol{e}_\kappa T = p_t^{\mathrm{T}} \boldsymbol{e}_\kappa T = p_{t_\kappa} T \tag{44}$$

and thus the shifted signals have the form

$$u_0(\boldsymbol{x} - \boldsymbol{X}_\kappa) = u_0(\boldsymbol{x}) \mathrm{e}^{-p_{t_\kappa} T} \quad \text{and} \quad i_0(\boldsymbol{x} - \boldsymbol{X}_\kappa) = i_0(\boldsymbol{x}) \mathrm{e}^{-p_{t_\kappa} T}. \tag{45}$$

As a result, an inductance approximated with the trapezoidal rule (40) is then described by $U_0 = Z_0 I_0$ with the impedance

$$Z_0(\psi_\kappa) = \psi_\kappa R_0, \quad R_0 = \frac{2L_0}{T}, \tag{46}$$

where we have made use of the complex equivalent frequency variable

$$\psi_\kappa = \frac{1 - e^{-p_{t_\kappa} T}}{1 + e^{-p_{t_\kappa} T}} = \tanh\left(\frac{p_{t_\kappa} T}{2}\right). \tag{47}$$

The obtained relationship implies the frequency approximation $p_{t_\kappa} \approx (2/T)\psi_\kappa$. Approximation of a respective capacitance leads to $Z_0(\psi_\kappa) = R_0/\psi_\kappa$ with R_0 as indicated before. As (47) maps the left and right half planes of p_{t_κ} to the left and right half planes of ψ_κ, respectively, stability properties of the continuous system are retained in the discrete approximation.

7.2.2. Generalization to LMS methods. Obtaining the wave digital algorithm for LMS methods other than the trapezoidal rule is feasibly performed in the frequency domain [20]. In analogy to (40), we start from a generalization of the usual time-domain definition to the multidimensional case, i.e. the finite difference scheme

$$\sum_{\sigma=0}^{s} \beta_\sigma u_0(\boldsymbol{x} - \sigma \boldsymbol{X}_\kappa) = \frac{L_0}{T} \sum_{\sigma=0}^{s} \alpha_\sigma i_0(\boldsymbol{x} - \sigma \boldsymbol{X}_\kappa), \quad \alpha_0 = 1, \tag{48}$$

DOI: 10.1002/jnm

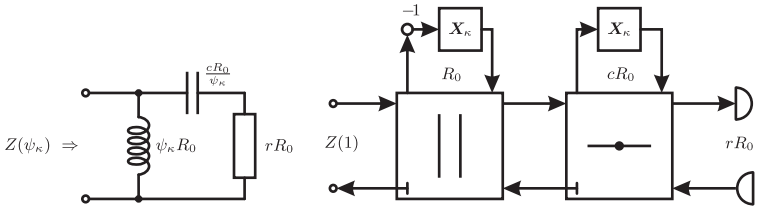

(a) (b)

method	r	c	q
Trapezoidal rule	0	0	2
Backward Euler	1	0	1
Gear	2	1	2

(c)

Figure 9. Approximation of an inductance: Passive 1-step ($c=0$) or 2-step ($c>0$) method, $r \geqslant 0$. (a) Reference circuit; (b) wave digital algorithm; and (c) well-known methods with consistency order q.

where α_σ and β_σ are real parameters of the method with s steps, assuming that α_s and β_s are not zero simultaneously. Switching to the frequency domain just as before leads to the characteristic impedance

$$Z(\psi_\kappa) = \frac{\sum_{\sigma=0}^{s} \alpha_\sigma (1-\psi_\kappa)^\sigma (1+\psi_\kappa)^{s-\sigma}}{2\sum_{\sigma=0}^{s} \beta_\sigma (1-\psi_\kappa)^\sigma (1+\psi_\kappa)^{s-\sigma}} R_0 \quad \text{with } R_0 = \frac{2L_0}{T}, \tag{49}$$

which was introduced in [21] for the one-dimensional case. We assume an irreducible method, i.e. the nominator and denominator have no common zeros. Furthermore, the method is passive, or synonymously A-stable, if and only if $Z(\psi_\kappa)$ is a Brune-function [20, 22]. The characteristic impedance of a passive method can be synthesized as an internally passive one-port, which serves as reference circuit for the derivation of a wave digital algorithm. Figure 9 shows an example including parameters for some well-known methods, where q denotes the consistency order as a measure of accuracy [14]. Degrees of freedom are chosen such that $s=q=2$ for $c>0$ and $s=1$, $q \leqslant 2$ for $c=0$. Notice that passive methods cannot exceed $q=2$. We emphasize that although passive LMS methods are inevitably implicit, the resulting wave digital algorithm of Figure 9 is explicit. To achieve this, the port resistance of the connecting port is necessarily equal to $Z(1)$, see [19].

8. WAVE DIGITAL ALGORITHM FOR THE FLUID DYNAMIC EQUATIONS

Figure 10 depicts the complete wave digital algorithm for the fluid dynamic equations corresponding to Figure 6, using the trapezoidal rule. For the special case (25), the realizations of the respective inductances can be omitted, as well as the series adaptor realizing $\mathscr{L}_\mathrm{d}$ if the series adaptor realizing $\mathscr{L}_\mathrm{b}$ is chosen to be unconstrainted [19].

Realizations of the reactive elements are shaded in gray. As an example, usage of a two-step LMS method instead of the trapezoidal rule amounts to substituting each shaded shift/inverter pair by the wave digital structure of Figure 9(b) together with the transformer regarding nonlinearity, while retaining the associated coordinate direction.

An abstract view of the algorithm is shown in Figure 11(a), which is comprised of the nonreactive part, and the reactive part depicted there for the trapezoidal rule. The algorithm needs to be computed for each point in a space–time grid. This grid is prescribed by the occurring shift vectors $\boldsymbol{X}_1$ and $\boldsymbol{X}_2$, and thus by the columns of the transformation matrix $\boldsymbol{H}$ and the chosen step size, cf. (41). Figure 11(b) depicts the resulting computation scheme: Nodes indicate the grid points, and arrows indicate the shifting of waves and thus information flow between the nodes. Owing to the special choice of $\boldsymbol{H}$, a regular checkerboard sampling is obtained. Memory storage can be done with two consecutive time layers, holding all nodes in space for one time instant. In particular, all the nodes in a time layer can be computed independent of one another by the knowledge of the waves from the previous time layer. The scheme thus exhibits a massive parallelism, which can efficiently be exploited on multicore processors [23].

Of course, the wave digital algorithm modeling the fluid dynamic equations is nonlinear: Element values—and thus port resistances—depend on field quantities, i.e. on both waves of the

DOI: 10.1002/jnm

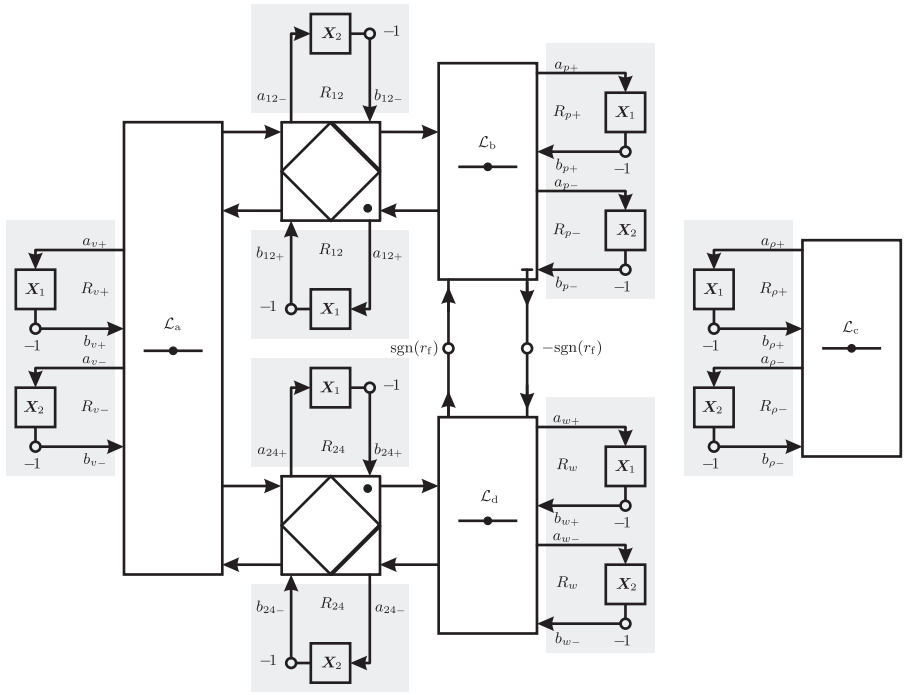

Figure 10. Wave digital algorithm for the fluid dynamic equations.

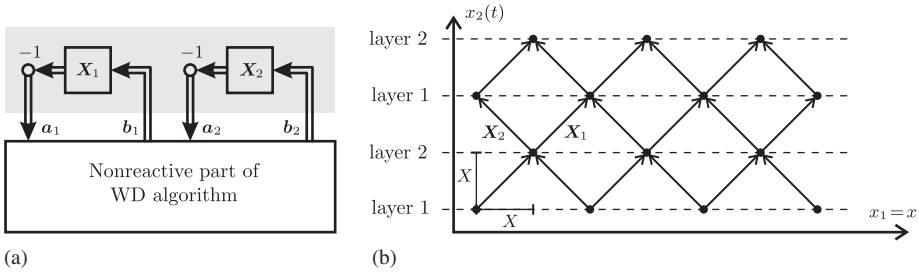

Figure 11. (a) Abstract view of the WD algorithm using the trapezoidal rule and (b) resulting space–time computation scheme.

reactive elements. Referring to Figure 11(a), we can globally describe the nonreactive part by a scattering matrix

$$\boldsymbol{b}(\boldsymbol{x}) = \boldsymbol{S}(\boldsymbol{a}(\boldsymbol{x}), \boldsymbol{b}(\boldsymbol{x}))\, \boldsymbol{a}(\boldsymbol{x}) \quad \text{with } \boldsymbol{a} = [\boldsymbol{a}_1^{\mathrm{T}}, \boldsymbol{a}_2^{\mathrm{T}}]^{\mathrm{T}} \quad \text{and} \quad \boldsymbol{b} = [\boldsymbol{b}_1^{\mathrm{T}}, \boldsymbol{b}_2^{\mathrm{T}}]^{\mathrm{T}}, \tag{50}$$

where waves are denoted with respect to the nonreactive part, not the reactive elements. The nonlinearity expresses itself in the dependence of the scattering matrix $\boldsymbol{S}$ on waves. For each individual node, we resolve the nonlinearity by a multidimensional fixed point iteration

$$\boldsymbol{b}_\nu(\boldsymbol{x}) = \boldsymbol{S}(\boldsymbol{a}(\boldsymbol{x}), \boldsymbol{b}_{\nu-1}(\boldsymbol{x}))\, \boldsymbol{a}(\boldsymbol{x}). \tag{51}$$

Incident waves $\boldsymbol{a}$ taken from the previous timestep remain fixed, whereas reflected waves $\boldsymbol{b}$ are calculated iteratively.

The complete computation scheme for one node is depicted in Figure 12. Comments on each block are in order.

1. Prepare to read/write waves from/to the proper grid points (acquire memory locations).
2. Waves incident to the algebraic part are obtained, i.e. $\boldsymbol{a}$ from (50). For LMS methods other than the trapezoidal rule, this involves computing part of the respective wave digital algorithm, cf. Figure 9(b).

DOI: 10.1002/jnm

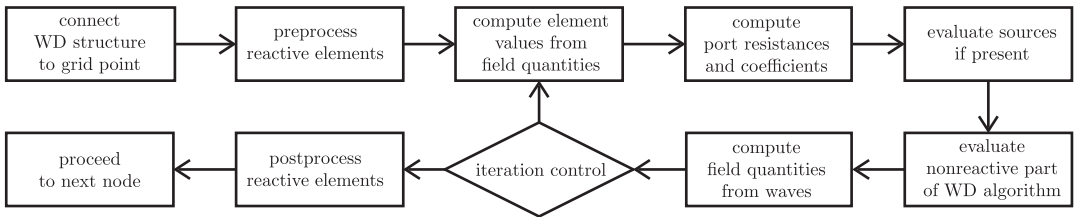

Figure 12. Program flow for each individual node.

3. All element values (28) are computed from field quantities, the values of which are taken from the previous iteration of this node.
4. All variant intermediate values necessary for evaluation of the algebraic part are computed, such as port resistances and adaptor coefficients.
5. Sources that depend on field quantities are evaluated in each iteration.
6. Evaluation of the nonreactive part results in the vector b_v of (51) for the iteration v.
7. Given the port resistances and the vectors $\boldsymbol{a}$, $\boldsymbol{b}_v$, updated values for the field quantities are computed.
8. Iteration control is performed using an *a posteriori* error estimation together with a predefined error bound.
9. Upon finishing the last iteration, the remaining part of the LMS wave digital algorithm is computed.

9. INITIAL AND BOUNDARY CONDITIONS

The wave digital algorithm as in Figure 10 models the given set of PDEs in the interior of a predefined computation domain. It needs to be complemented by an algorithm producing the missing waves at the temporal and spatial boundaries. This usually involves expressing initial and boundary conditions for the field quantities in terms of wave variables. In [24], we have presented a generic algorithm for the wave initialization of passive LMS methods, which performs several steps with a one-step method and subsequently employs a state estimation. Using this algorithm, implementation of initial and boundary conditions is done with a suitable one-step method, and switching to an arbitrary passive LMS method can then be performed independent of the physical problem.

In the present case, we use the half-step evaluation [4] for implementation of the initial conditions, which leads to expressions as

$$\begin{aligned} b_{v+}(\boldsymbol{x_n}) &= -\tfrac{1}{2}(\sqrt{R_{v+}}\, i_1)(\boldsymbol{x_n} - \boldsymbol{X}_1/2), \\ b_{v-}(\boldsymbol{x_n}) &= -\tfrac{1}{2}(\sqrt{R_{v-}}\, i_1)(\boldsymbol{x_n} - \boldsymbol{X}_2/2), \\ b_{12+}(\boldsymbol{x_n}) &= -\tfrac{1}{2}(\sqrt{R_{12}}[i_1 + i_2])(\boldsymbol{x_n} - \boldsymbol{X}_1/2), \\ b_{12-}(\boldsymbol{x_n}) &= -\tfrac{1}{2}(\sqrt{R_{12}}[i_1 - i_2])(\boldsymbol{x_n} - \boldsymbol{X}_2/2) \end{aligned} \tag{52}$$

etc. Values on the right-hand side can be computed from initial conditions for v, p, ρ and w using (21), the respective scale functions from Section 6.6, the element values (28) and the relationship $R = 2L/T$.

We have implemented a hard boundary using a symmetry argument [10], which imposes the conditions

$$\begin{aligned} v(x_\mathrm{b}+0,t) &= -v(x_\mathrm{b}-0,t), \quad & p(x_\mathrm{b}+0,t) &= p(x_\mathrm{b}-0,t), \\ \rho(x_\mathrm{b}+0,t) &= \rho(x_\mathrm{b}-0,t), \quad & w(x_\mathrm{b}+0,t) &= w(x_\mathrm{b}-0,t). \end{aligned} \tag{53}$$

DOI: 10.1002/jnm

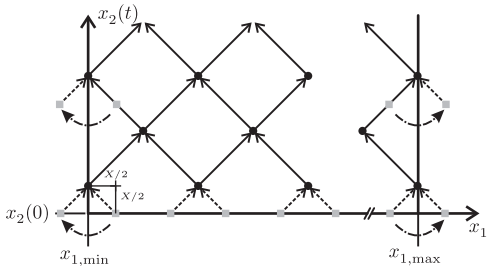

Figure 13. Computation scheme accounting for half-step initialization.

Using the half-step evaluation, this allows the formulation of the missing waves in terms of already computed waves from inside the computation domain, i.e.

$$\begin{aligned} b_{v+}(\boldsymbol{x}_\mathrm{b}) &= -\,b_{v-}(\boldsymbol{x}_\mathrm{b}), \quad b_{p+}(\boldsymbol{x}_\mathrm{b}) = b_{p-}(\boldsymbol{x}_\mathrm{b}), \quad b_{\rho+}(\boldsymbol{x}_\mathrm{b}) = b_{\rho-}(\boldsymbol{x}_\mathrm{b}), \\ b_{12+}(\boldsymbol{x}_\mathrm{b}) &= -\,b_{12-}(\boldsymbol{x}_\mathrm{b}), \quad b_{24+}(\boldsymbol{x}_\mathrm{b}) = -b_{24-}(\boldsymbol{x}_\mathrm{b}). \end{aligned} \tag{54}$$

At the left boundary, waves on the left-hand side are missing, and at the right boundary, waves on the right-hand side are missing, respectively. Figure 13 shows the resulting computation scheme with a sampling offset of half a step size from the temporal boundary.

10. NUMERICAL EXAMPLES

We adopt the well-known benchmark problem of a shock tube for the frictionless case $\eta = 0$, which is defined by the initial conditions

$$\begin{aligned} v(x,0) &= v_0 + (v_1 - v_0)\mathrm{u}(x - x_0), \quad p(x,0) = p_0 + (p_1 - p_0)\mathrm{u}(x - x_0), \\ \rho(x,0) &= \rho_0 + (\rho_1 - \rho_0)\mathrm{u}(x - x_0), \end{aligned} \tag{55}$$

where u is the unit step function. The analytical solution to this problem is known [13]. It is a so-called weak solution as it contains discontinuities spatially moving with evolving time. This constitutes a crucial difficulty for the numerical integration, as the assumption of continuity for the theory of LMS methods is violated. This holds also for initialization formulas such as the half-step evaluation.

The initial values are chosen to be $v_0 = v_1 = 0$, $p_0 = 10^5\,\mathrm{N/m^2}$, $p_1 = 10^4\,\mathrm{N/m^2}$, $\rho_0 = 1\,\mathrm{kg/m^3}$ and $\rho_1 = 0.125\,\mathrm{kg/m^3}$. Regarding (18d), we obtain $w(x,0) = 0$ as remaining initial condition. We choose $p_\mathrm{f} l_\mathrm{f} = \frac{1}{2}$ according to (33) and a hyperbolization constant of $l_\mathrm{f} = 10^{-5}$, such that the corresponding term in (31) does not dominate. Furthermore, the step size is $X = 10^{-3}\,\mathrm{m}$ and the simulation ends at $t_\mathrm{e} = 5 \cdot 10^{-4}\mathrm{s}$. For simplicity, we choose a constant time scale

$$v_2 = \frac{X[N - 0.5]}{t_\mathrm{e}}, \tag{56}$$

which regards the half-step initialization. With a number of time steps $N = 1000$, the value of v_2 satisfies (31) according to the analytical solution. For the resolution of nonlinearities via (51), the wave digital realization corresponding to Figure 5(a) leads to a smaller Lipschitz constant and thus faster convergence for approximately $\eta < 10^{-1}\,\mathrm{Ns\,m^{-2}}$, whereas the realization corresponding to Figure 5(b) performs better for $\eta \geqslant 10^{-1}\,\mathrm{Ns\,m^{-2}}$. As the range of interest is the former one in this case, we have used the respective realization. The iteration control of Figure 12 requires at least two iterations per node, and using a relative error bound of $\varepsilon = 10^{-4}$ for resolving the nonlinearity resulted in an average of 2.2 iterations per node for all of the following examples.

Figure 14 shows the simulation results for vanishing friction, $\eta = 0$, using the trapezoidal rule. It exhibits the known unwanted oscillations due to the discontinuities, which render the numerical solution useless [10, 12, 15]. In Figure 15, the results are shown for $\eta = 10^{-1}\,\mathrm{Ns\,m^{-2}}$ still using the trapezoidal rule. Most of the oscillations are suppressed as the friction softens the shock. It shall be noted that this is only possible for reasonably high values of η, or, respectively,

DOI: 10.1002/jnm

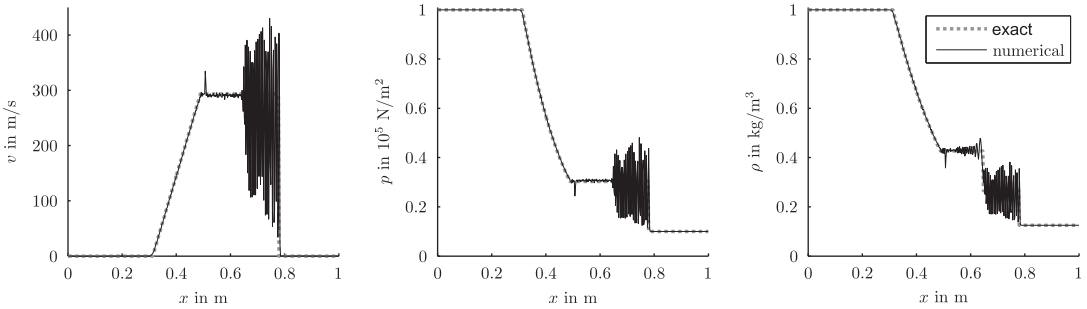

Figure 14. Simulation results using the trapezoidal rule, with $\eta = 0$ (frictionless case).

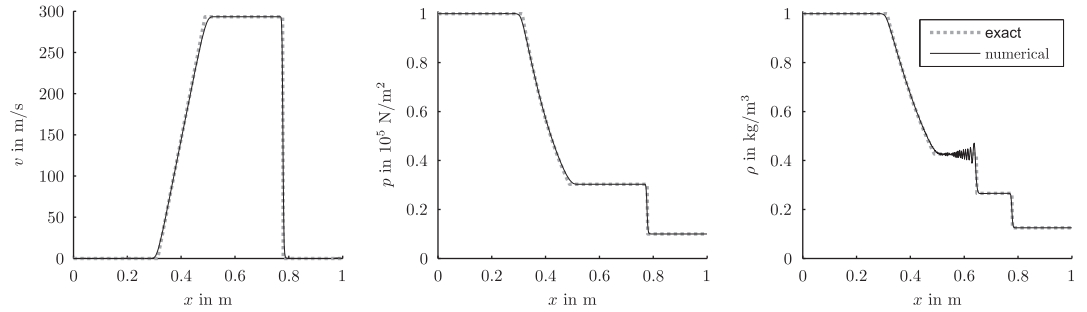

Figure 15. Simulation results using the trapezoidal rule, with $\eta = 10^{-1}\,\mathrm{Ns\,m^{-2}}$.

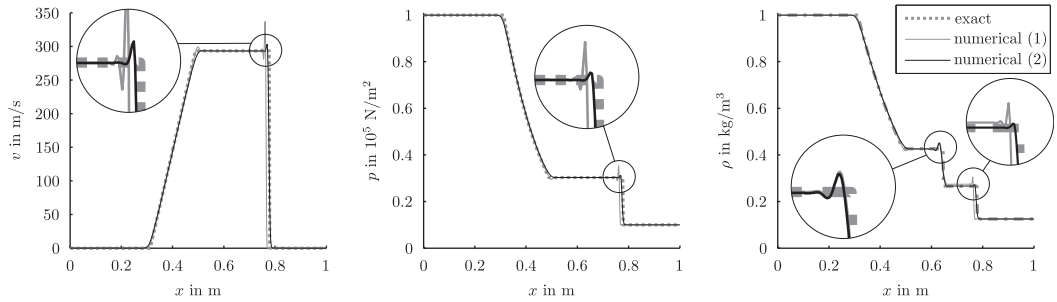

Figure 16. Simulation results using the Gear method, with $\eta = 0$ (1) and $\eta = 10^{-1}\,\mathrm{Ns\,m^{-2}}$(2), respectively.

small enough step sizes X. More specifically, the width of the softened shock is proportional to η [12], and a reduction of η by a factor of 10 requires the step size to be chosen 10 times smaller to still suppress oscillations, which increases the overall computational effort by factor 100 as the number of dimensions is $k = 2$ (space and time). Moreover, the contact discontinuity of the density ρ still produces oscillations. This was to be expected as the velocity is constant in this range, such that there is no friction. According to Mengel [12], these oscillations can further be suppressed by a deeper physical model accounting for heat conduction.

Similar to the approach of Hetmanczyk and Ochs [15], we used the Gear method to obtain the results of Figure 16. Additional losses are now introduced by the integration method itself, and oscillations are suppressed regardless of the presence of friction. For the frictionless case, overshoots occur at discontinuities and there is a small spatial offset of the shock position. This effect is significantly reduced when friction is present. Even though the wave digital algorithm is more complex using the Gear method, solutions of reasonable quality can be obtained with a computation time much less than for the trapezoidal rule, as a larger step size can be used. For the dynamic viscosities $\eta = 10^{-1}\,\mathrm{Ns\,m^{-2}}$ (olive oil), $\eta = 10^{-2}\,\mathrm{Ns\,m^{-2}}$ and $\eta = 10^{-3}\,\mathrm{Ns\,m^{-2}}$ (water), a step size of $X = 10^{-3}\,\mathrm{m}$ can be maintained for suppressing oscillations, whereas in case of the trapezoidal rule the step sizes $X = 10^{-3}\,\mathrm{m}$, $X = 10^{-4}\,\mathrm{m}$ and $X = 10^{-5}\,\mathrm{m}$ are necessary,

DOI: 10.1002/jnm

respectively, to obtain results as in Figure 15. This leads to the ratios 0.74, 74 and 7400 of computation time, not considering specific optimizations as local step size variation, which is a vast problem on its own.

Some comments on standard fluid dynamic terminology are in order. The wave digital algorithm using Gear's LMS method is second-order accurate in space–time. The scheme is not monotonicity preserving and thus not total variation diminishing (TVD) or monotone, which is reflected by the occurrence of new local extrema around the discontinuities. However, the reference circuit converges to the frictionless case in a continuous fashion as $\eta \to 0$, thus of all weak solutions the algorithm appears to select the desired vanishing-viscosity solution quite naturally. To obtain the TVD property, a standard approach in fluid dynamics is the usage of some sort of nonlinear flux/slope-limiting algorithm for steep transitions additionally to the integration method. This should be possible in the wave digital algorithm as well; however, we do not pursue this path as this is beyond the scope of this paper. Rather, we have presented a network theoretical approach to introduce artificial losses suppressing high-frequency content.

11. CONCLUSIONS

We have revisited the wave digital method for numerical integration of PDEs from a general, but application-oriented point of view. The step-by-step approach for the synthesis of reference circuits is applicable to many different PDEs, and to models with more than one spatial coordinate. By using the differential operator and its properties, derivations are simplified appreciably.

Once a reference circuit is obtained, it can schematically be expanded to use passive LMS methods other than the trapezoidal rule. Despite the superior stability and accuracy properties of the trapezoidal rule, for specific problems it can be very beneficial to introduce lossy integration methods like the Gear method, e.g. to suppress oscillations when discontinuities are present. Whenever a deeper physical modeling is not viable or not wanted, this approach offers a generic solution as it is independent of the exact physical nature of the problem. For the shock tube problem, we have shown that meaningful simulation may be possible with a step size much larger than when using the trapezoidal rule, which significantly reduces computation time.

REFERENCES

1. Fettweis A, Nitsche G. Numerical integration of partial differential equations using principles of multidimensional wave digital filters. *Journal of VLSI Signal Processing* 1991; **3**(1/2):7–24.
2. Fettweis A, Nitsche G. Transformation approach to numerically integrating PDEs by means of WDF principles. *Multidimensional Systems and Signal Processing* 1991; **2**(2):127–159.
3. Fettweis A. The role of passivity and losslessness in multidimensional digital signal processing—new challenges. *Proceedings of the IEEE International Symposium on Circuits and Systems* (*ISCAS*), Singapore, vol. 1, June 1991; 112–115.
4. Fettweis A. Robust numerical integration using wave-digital concepts. *Multidimensional Systems and Signal Processing* 2006; **17**(1):7–25.
5. Ochs K. Wave digital simulation of passive systems in linear state-space form. *International Journal for Numerical Modelling*: *Electronic Networks, Devices and Fields* 2010; **23**(1): 42–61.
6. Leuer C, Ochs K. Systematic derivation of reference circuits for wave digital modeling of passive linear partial differential equations. *Proceedings of the 52nd IEEE 2009 Midwest Symposium on Circuits and Systems* (*MWSCAS*), Cancun, Mexico, August 2009; 782–785.
7. Hemetsberger G. Numerische Integration hyperbolischer partieller Differentialgleichungen unter Verwendung mehrdimensionaler Wellendigitalfilter. *Doctoral Thesis*, Ruhr-University Bochum, 1995.
8. Fettweis A. Discrete modelling of lossless fluid dynamic systems. *International Journal of Electronics and Communications* (AEÜ) 1992; **46**(4):209–218.
9. Fettweis A. Improved wave-digital approach to numerically integrating the PDEs of fluid dynamics. *Proceedings of the 2002 IEEE International Symposium on Circuits and Systems* (*ISCAS*), Scottsdale, AZ, USA, vol. 3, May 2002; 361–364.
10. Fries M. Numerical integration of Euler flow by means of multidimensional wave digital principles. *Doctoral Thesis*, Ruhr-University, Bochum, 1995.
11. Fettweis A. *Unpublished Notes*, 2000–2009.
12. Mengel A. Untersuchungen zur numerischen Lösung der Navier–Stokes Gleichungen mit Wellendigital-Prinzipien. *Doctoral Thesis*, Ruhr-University, Bochum, 2007.
13. Hirsch C. *Numerical Computation of Internal and External Flows*, vol. 1/2. Wiley: New York, 1990.
14. Dahlquist G. A special stability problem for linear multistep methods. *BIT* 1963; **3**:27–43.

DOI: 10.1002/jnm

15. Hetmanczyk G, Ochs K. Wave digital simulation of Burgers' equation using Gear's method. *Proceedings of the 51st IEEE 2008 Midwest Symposium on Circuits and Systems* (*MWSCAS*), Knoxville, TN, USA, August 2008; 161–164.
16. Willems JL. *Stability Theory of Dynamical Systems*. Nelson: London, 1970.
17. Fränken D, Meerkötter K, Wassmuth J, Observer-based feedback linearization of dynamic loudspeakers with AC amplifiers. *IEEE Transactions on Speech and Audio Processing* 2005; **13**(2):233–242.
18. Meerkötter K, Felderhoff T. Simulation of nonlinear transmission lines by wave digital filter principles, *Proceedings of the IEEE International Symposium on Circuits and Systems*, San Diego, CA, USA, May 1992; 875–878.
19. Fettweis A. Wave digital filters: theory and practice. *Proceedings of the IEEE* 1986; **74**(2):270–327.
20. Fischer HD. Wave digital filters for numerical integration. *ntz-Archiv* 1984; **6**(2):37–40.
21. Ochs K. Passive integration methods: fundamental theory. *International Journal of Electronics and Communications* (AEÜ) 2001; **55**(3):153–163.
22. Belevitch V. *Classical Network Theory*. Holden-Day: San Francisco, 1968.
23. Hetmanczyk G. Exploiting the parallelism of multidimensional wave digital algorithms on multicore computers. *Multidimensional Systems and Signal Processing* 2010; **21**(1):45–58.
24. Hetmanczyk G, Ochs K. Initialization of linear multistep methods in multidimensional wave digital models. *Proceedings of the 52nd IEEE 2009 Midwest Symposium on Circuits and Systems* (*MWSCAS*), Cancun, Mexico, August 2009; 786–789.

AUTHORS' BIOGRAPHIES

Georg Hetmanczyk was born in Bochum, Germany, in 1979. He studied at the Purdue-University, IN, USA, and the Ruhr-University, Bochum, Germany, where he received his Diplom-Ingenieur degree in 2006. Since then, he has been with the Chair of Communications Engineering at the Ruhr-University, where he is now working towards a doctoral degree. His current research interests include multidimensional digital signal processing and numerical integration of partial differential equations.

He received a scholarship from the German Academic Exchange Service (DAAD) in 2004, the scholarship of Prof. Dr. Koepchen Studienstiftung of the RWE 2004–2006, and is a stipendiary of e-fellows.net since 2004. He is a member of the Research School at Ruhr-University Bochum.

Karlheinz Ochs was born in Lingen, Germany, in 1968. He received the Dipl.-Ing. degree and the Dr.-Ing. degree in Electrical Engineering both from the University of Paderborn, Germany, in 1996 and 2001, respectively. From 2001 to 2002, he was a design engineer at the Technology and Development Center, Siemens AG, Bruchsal, Germany. Currently, he is a postdoctoral researcher at the Department of Electrical Engineering and Information Technology/Communications Engineering at the Ruhr-University, Bochum, Germany. His research interests include digital signal processing and transmission.

DOI: 10.1002/jnm